# Electric properties and phase transition behavior in lead lanthanum zirconate stannate titanate ceramics with low zirconate content*

Zeng Tao(曾 涛)[a)†], Lou Qi-Wei(漏琦伟)[a)], Chen Xue-Feng(陈学锋)[b)‡], Zhang Hong-Ling(张红玲)[c)], Dong Xian-Lin(董显林)[b)], and Wang Gen-Shui(王根水)[b)]

[a)] *Shanghai Key Laboratory of Materials Protection and Advanced Materials in Electric Power, Shanghai University of Electric Power, Shanghai* 200090, *China*

[b)] *Key Laboratory of Inorganic Functional Materials and Devices, Shanghai Institute of Ceramics, Chinese Academy of Sciences, Shanghai* 200050, *China*

[c)] *National Engineering Laboratory for Hydrometallurgical Cleaner Production Technology, Institute of Process Engineering, Chinese Academy of Sciences, Beijing* 100190, *China*

(Received 23 March 2015; revised manuscript received 19 May 2015; published online 9 October 2015)

The phase transitions, dielectric properties, and polarization versus electric field (*P*–*E*) hysteresis loops of $Pb_{0.97}La_{0.02}(Zr_{0.42}Sn_{0.58-x}Ti_x)O_3$ ($0.13 \leq x \leq 0.18$) (PLZST) bulk ceramics were systematically investigated. This study exhibited a sequence of phase transitions by analyzing the change of the *P*–*E* hysteresis loops with increasing temperature. The antiferroelectric (AFE) to ferroelectric (FE) phase boundary of PLZST with the Zr content of 0.42 was found to locate at the Ti content between 0.14 and 0.15. This work is aimed to improve the ternary phase diagram of lanthanum-doped PZST with the Zr content of 0.42 and will be a good reference for seeking high energy storage density in the PLZST system with low-Zr content.

**Keywords:** PLZST ceramics, ferroelectricity, antiferroelectricity, phase transition

**PACS:** 77.80.–e, 77.80.B–, 77.84.Cg **DOI:** 10.1088/1674-1056/24/11/117702

## 1. Introduction

The lead zirconate stannate titanate [Pb(Zr,Sn,Ti)$O_3$, or PZST] system including lanthanum-doped PZST (PLZST) has been widely investigated for applications as charge-storage capacitors, transducers, actuators, etc[1–8] since Berlincourt established the ternary phase diagram of PZST in the 1960s, as shown in Fig. 1.[9] In particular, the antiferroelectric (AFE)/ferroelectric (FE) phase boundary in PLZST has been mostly studied for obtaining a high energy storage density. Markowski *et al.*[5] evaluated the effect of compositional modifications on the electrical properties of $(Pb_{0.98}La_{0.02})(Zr_{0.66}Sn_{0.36-x}Ti_x)O_3$ ($x = 0.07$, 0.08, 0.09, 0.10, 0.11) (shown as S1–S5 in Fig. 1) and $(Pb_{0.98}La_{0.02})(Zr_{0.9-x}Sn_xTi_{0.1})O_3$ ($x = 0.3$, 0.25, 0.2, 0.15, 0.1) (shown as B1–B5 in Fig. 1) ceramics. They found that with $Ti^{4+}$ content increasing in S1–S5 ceramics or $Zr^{4+}$ content increasing in B1–B5 ceramics, the switching field decreased while the AFE–FE transition temperature increased. Some other researchers, including Mirshekarloo,[10] Forst,[11] and Frederick,[12] also confirmed that when the ratio of Sn/Ti or Sn/Zr increased, the AFE phase was stabilized. Recently, Wang *et al.*[13] obtained a relatively high energy storage density in the $Pb_{0.97}La_{0.02}(Zr_{0.9}Sn_{0.05}Ti_{0.05})O_3$ ceramics.

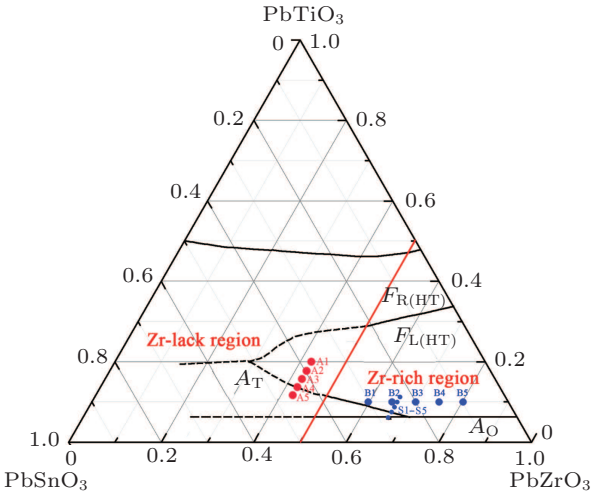



**Fig. 1.** (color online) Room temperature phase diagram of ternary system $PbTiO_3$–$PbZrO_3$–$PbSnO_3$.

The previous investigations almost concentrated on the high-Zr region where the Zr content is above 0.50. As a matter of fact, when the Zr content is lower than 0.50, PLZST ceramics such as $Pb_{0.97}La_{0.02}(Zr_{0.42}Sn_{0.4}Ti_{0.18})O_3$ also exhibit some interesting performance.[14,15] Zhang *et al.*[14] detected a relatively high pyroelectric coefficient in $Pb_{0.97}La_{0.02}(Zr_{0.42}Sn_{0.40}Ti_{0.18})O_3$ ceramics due to the electric-field-induced ferroelectric ($FE_{IN}$) to AFE phase transition in the poled sample and obtained a high reversible max-

*Project supported by the National Natural Science Foundation of China (Grant Nos. 51202273, 11204304, and 11304334) and the Science and Technology Commission of Shanghai Municipality, China (Grant No. 14DZ2261000).

†Corresponding author. E-mail: zengtao@shiep.edu.cn

‡Corresponding author. E-mail: xfchen@mail.sic.ac.cn

© 2015 Chinese Physical Society and IOP Publishing Ltd 

imum pyroelectric response with a dc bias applying on the depoled sample. Recently, Chen *et al.*[16] investigated the effect of La doping on the phase transition in $Pb(Zr_{0.42}Sn_{0.4}Ti_{0.18})O_3$ by Raman scattering. However, compared with the PLZST system with Zr content above 0.5, there is relative little research on the PLZST system with low Zr content. When the Zr content is below 0.50, the phase transition behavior of the PZST system is not clear. So the phase diagram in the Zr-low region is blank, as seen in Fig. 1.

To seek a high energy storage density in the PZST system with low-Zr content, it is necessary to investigate the variation of the polarization versus electric field (*P*–*E*) hysteresis loops with the change of the Sn:Ti ratio in the Zr-low region. In this study, we investigate the phase transitions, dielectric properties, and *P*–*E* hysteresis loops of $Pb_{0.97}La_{0.02}(Zr_{0.42}Sn_{0.58-x}Ti_x)O_3$ ceramics with various Sn:Ti ratios. The compositions selected in this research are shown in Fig. 1, where A1, A2, A3, A4, and A5 correspond to $x = 0.18$, $x = 0.16$, $x = 0.15$, $x = 0.14$, and $x = 0.13$, respectively. This work improves the ternary phase diagram of lanthanum-doped PZST with the Zr content of 0.42 and is a good reference for seeking high energy storage density in the PLZST system with low-Zr content.

## 2. Experimental procedure

The $Pb_{0.97}La_{0.02}(Zr_{0.42}Sn_{0.58-x}Ti_x)O_3$ bulk ceramics with $0.13 \leq x \leq 0.18$ were fabricated using the conventional ceramic process. The starting raw materials were $Pb_3O_4$ (97.43%), $ZrO_2$ (99.87%), $TiO_2$ (99.38%), $SnO_2$ (99.5%), and $La_2O_3$ (99%). They were mixed stoichiometrically, and 0.5 wt.% excess $Pb_3O_4$ was added considering the volatilization of PbO during sintering. Aqueous suspensions of all raw materials were ball-milled for 6 h and dried at 120 °C. The dried powder was then calcined at 850 °C for 2 h and ball-milled again for 24 h. After drying, about 6 wt.% PVA was mixed with the powder, and the mixture was crushed to pass through a 30-mesh sieve. Then the powder was pressed into disks of 15 mm diameter. Following binder burnout at 800 °C, the pellets were put in a sealed crucible filled with powder of the same composition, and sintered at about 1320 °C for 1 h.

The fresh bulk ceramics were fabricated as disks with a diameter of 10 mm and a thickness of 1 mm, and silver electrodes were attached to both sides of the disks for electrical measurements. The crystal phases of the specimens were examined by x-ray diffraction ( XRD, D/max2550V; Rigaku, Tokyo, Japan) using Cu $K\alpha$ radiation. The temperature-dependent dielectric properties at 1 kHz were measured using an HP4284A LCR meter (Hewlett-Packard, Kobe-shi, Japan). The *P*–*E* hysteresis loops at 10 Hz were obtained by aix ACCT TF Analyzer 2000 (aix ACCT Co., Aachen, Germany).

## 3. Results and discussion

Figure 2(a) displays the XRD patterns of five PLZST samples at room temperature (RT). The patterns show high similarity to those of single powder,[17] suggesting a pure perovskite structure in all specimens. Moreover, A5 and A4 have a tetragonal structure as mainly evidenced by the split of (200) and (002) peaks over the $2\theta$ range from 44° to 45°, as shown in Fig. 2(b). These two peaks of the tetragonal phase are combined into one peak indicating the formation of the rhombohedral phase in A3, A2, and A1.

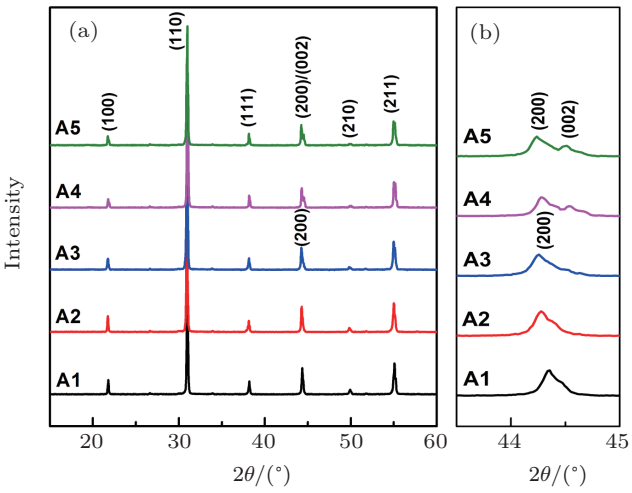



**Fig. 2.** (color online) XRD patterns of PLZST bulk ceramics with different Sn:Ti ratios.

There are two dielectric constant peaks in A1 ceramic shown in Fig. 3. One is at 110 °C, and the other is at 130 °C. The FE squared loop changes into an AFE double loop when the temperature increases to 110 °C, and then into a linear loop as the temperature further increases above 150 °C. Zhang *et al.*[14] also reported that the *P*–*E* hysteresis loops of A1 ceramics exhibit a typical FE character at RT, with the first loop inside the second one. The $P_r$ and $E_c$ decrease as the temperature increases, but all *P*–*E* hysteresis loops exhibit the typical FE character as long as the temperature is lower than 100 °C. When the temperature reaches about 110 °C, the first loop is outside of the second one, which indicates the AFE-induced ferroelectric phase ($FE_{IN}$) transition induced by the electric field.

There are two dielectric constant peaks in A2 ceramics shown in Fig. 4. One is at 80 °C, and the other is at 127 °C. The *P*–*E* hysteresis loops exhibit the typical FE character at 30 °C. The $P_r$ and $E_c$ are 25.4 μC/cm$^2$ and 0.57 kV/mm, respectively. As the temperature increases up to 80 °C, $P_r$ and $E_c$ decrease quickly and a slight AFE-like *P*–*E* hysteresis loop appears, which is caused by the phase transition of FE to AFE. So the first dielectric constant peak can be attributed to the FE–AFE phase transition. When the temperature rises up to 110 °C, the *P*–*E* hysteresis loops exhibit the typical AFE character. As the temperature further increases to 127 °C and above, the *P*–*E*

hysteresis loop changes into a linear loop, and $P_r$ and $E_c$ become zero, which demonstrate that the second dielectric constant peak is caused by the AFE-PE phase transition. Similar results have been found in A1 ceramics.

The dielectric constant versus temperature of A3 ceramics is shown in Fig. 5. The *P*–*E* hysteresis loops exhibit the typical FE character at 30 °C. As the temperature increases up to 55 °C, a slight AFE-like *P*–*E* hysteresis loop appears, while the dielectric constant peak is weak and almost invisible, which indicates only a few FE changes to AFE. This phenomenon demonstrates that with an increase in the Sn content, the FE content decreases and the AFE content increases gradually. This can be attributed to the Sn doping stabilizing the AFE phase.[18] With a further increase in temperature up to the Curie point, the *P*–*E* hysteresis loop of A3 ceramics also changes into a linear one.

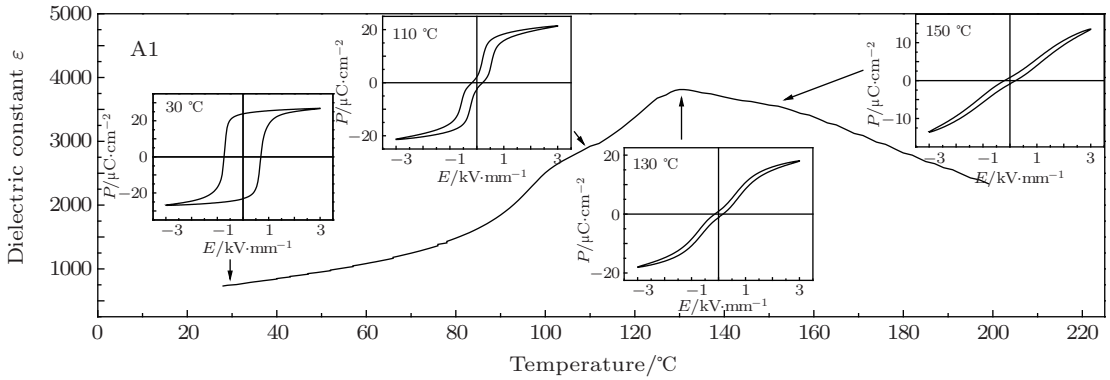



**Fig. 3.** Dielectric constant versus temperature of A1 ceramics; insets show *P*–*E* loops at different temperatures.

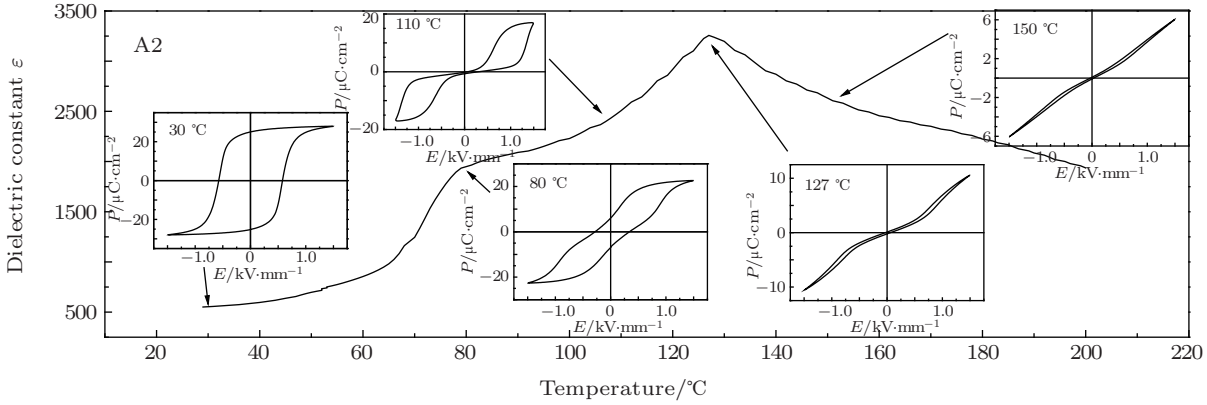



**Fig. 4.** Dielectric constant versus temperature of A2 ceramics; insets show *P*–*E* loops at different temperatures.

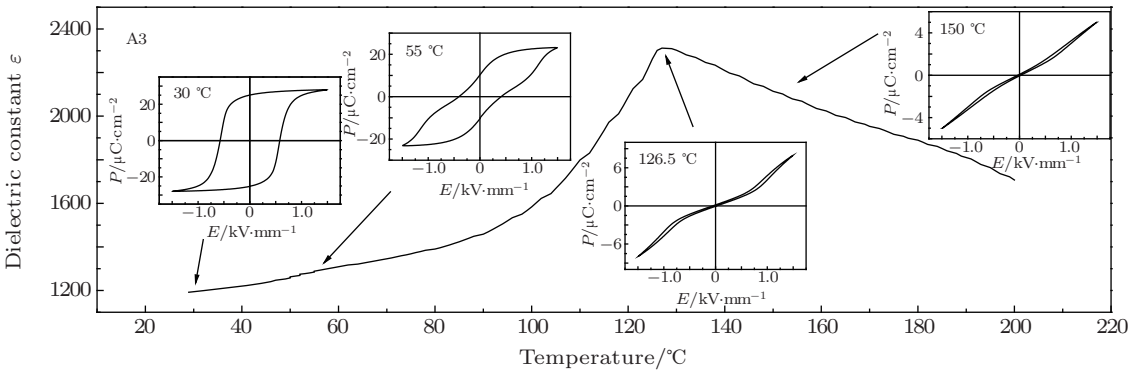



**Fig. 5.** Dielectric constant versus temperature of A3 ceramics; insets show *P*–*E* loops at different temperatures.

The dielectric constant as a function of temperature for A4 ceramics and the *P*–*E* loops are given in Fig. 6. There is only one dielectric peak in A4 ceramics due to the only AFE–PE phase transition. The forward-switching ($E_F$) and back-switching ($E_A$) fields are 1.94 kV/mm and 0.28 kV/mm at room temperature. When the temperature increases to 80 °C, $E_F$ and $E_A$ increase to 2.58 kV/mm and 2.08 kV/mm, respectively. The reason is that the FE phase induced from AFE

phase by the applied electric field is unstable and easy to recover to the AFE phase at $E_A$. As a result, when the temperature increases, a higher applied electric field is needed to stabilize the FE phase, which hence causes higher $E_F$ and $E_A$. The $\Delta E(=E_F-E_A)$ represents the thermal stability of the induced FE phase.[19] When the temperature increases, the FE phase becomes unstable, so $\Delta E$ decreases and the hysteresis loops become slimmer.

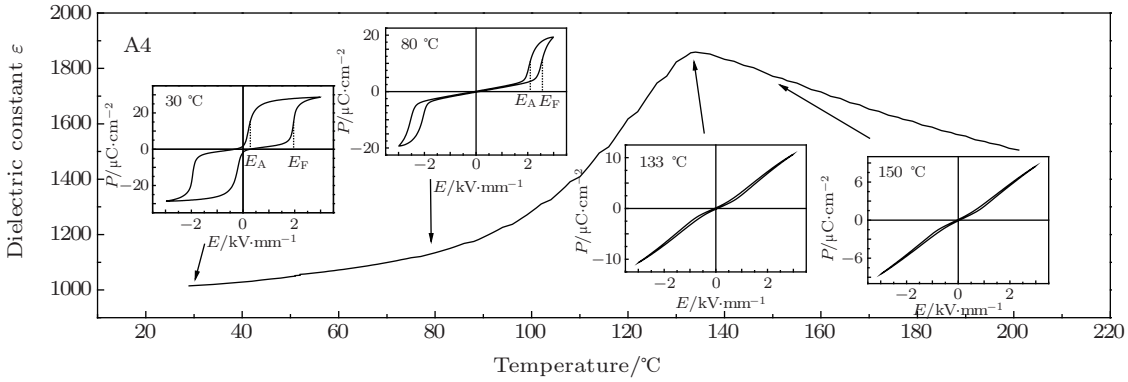



**Fig. 6.** Dielectric constant versus temperature of A4 ceramics; insets show *P*–*E* loops at different temperatures.

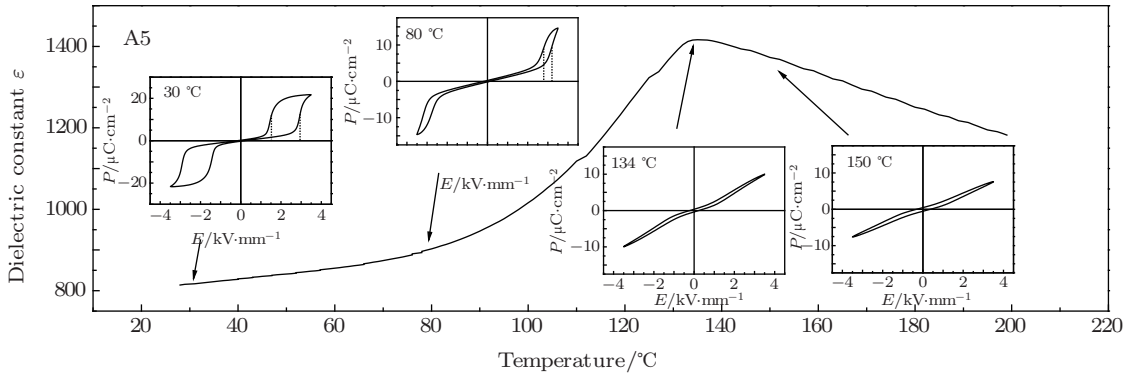



**Fig. 7.** Dielectric constant versus temperature of A5 ceramics; insets show four *P*–*E* loops taken at different temperatures.

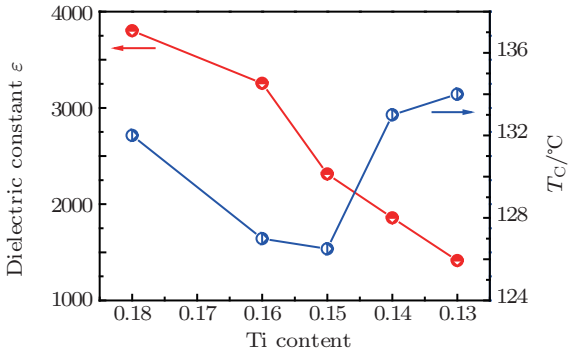



**Fig. 8.** (color online) Dependences of $\varepsilon$ and $T_C$ on Ti content of PLZST ceramics.

It can be known from the hysteresis loops of A3 and A4 ceramics at room temperature that FE phase PLZST changes to AFE phase PLZST with a decrease in the content of $Ti^{4+}$ from 0.15 to 0.14, which indicates that an FE/AFE phase boundary exists at the Ti content between 0.14 and 0.15.

Similar to A4 ceramics, A5 ceramics also exhibit one dielectric constant peak as shown in Fig. 7. The $E_F$ and $E_A$ are 2.94 kV/mm and 1.45 kV/mm larger than those of A3 ceramics, which indicates a relatively high amount of AFE phase in PLZST and a high energy storage density in this region. As the temperature increases, the double loop of A4 ceramics becomes slimmer and gradually loses its double hysteresis behavior, and changes into a linear loop at about 134 °C.

From the results of A1–A5 ceramics, the dependences of $\varepsilon$ and the Curie temperature $T_C$ on the Ti content for the PLZST ceramics are shown in Fig. 8. It can be observed that $\varepsilon_{max}$ decreases with decreasing Ti content. This can be attributed to the replacement of $Ti^{4+}$ ions (0.068 nm) by $Sn^{4+}$ (0.071 nm) ions leading to a decreasing $c/a$, and then eliminating the polarization contribution to the dielectric constant. It can also be seen from Fig. 8 that $T_C$ first drops with decreasing Ti content and then increases with Ti content decreasing lower than 0.15. With a drop in the Ti content, the FE long-range order is destroyed and the FE–PE phase transition temperature decreases. When the Ti content is at or just below 0.15, the AFE short-range order begin to establish and an FE to AFE phase transition occurs.[20] With a further decrease in the Ti content, the AFE phase becomes more stable, so the

AFE to PE phase transition temperature increases. This result demonstrates that the lowest $T_C$ exists at the FE to AFE phase transition boundary with the Ti content at or just below 0.15, which is consistent with the phase boundary result from the *P*–*E* loop.

## 4. Conclusion

The effect of the Sn:Ti ratio varying from 40:18 to 45:13 on the phase structure and electrical properties of $Pb_{0.97}La_{0.02}(Zr_{0.42}Sn_{0.58-x}Ti_x)O_3$ ceramics has been investigated. FE phase PLZST changes to AFE phase PLZST with a decrease in the Ti content from 0.15 to 0.14, which indicates that an FE/AFE phase boundary exists at the Ti content between 0.14 and 0.15. With a further decrease in the Ti content, the AFE phase in PLZST becomes more stable, and the back-switching fields increase, which indicates a high potential energy storage density in this region. With a decrease in the Ti content, the FE long-range order is destroyed and the FE–PE phase transition temperature decreases. With a further decrease in the Ti content, the AFE phase becomes more stable, so the AFE to PE phase transition temperature increases. This result demonstrates that the lowest $T_C$ exists at the FE to AFE phase transition boundary with a Ti content at or just below 0.15, which is consistent with the phase boundary result from the *P*–*E* loop.

## References


[1] Xu B M, Ye Y H and Cross L E 2000 *J. Appl. Phys.* **87** 2507
[2] Zhou L J, Zhao Z and Zimmermann A 2004 *J. Am. Ceram. Soc.* **87** 606
[3] Zhou L J, Rixecker G, Zimmermann A, Aldinger E, Zhao Z and Nygren M 2005 *J. Am. Ceram. Soc.* **88** 2952
[4] Wang D W, Zhang D Q, Yuan J, Zhao Q L, Liu H M, Wang Z Y and Cao M S 2009 *Chin. Phys. B* **18** 2596
[5] Markowski K, Park S E, Yoshikawa S and Cross L E 1996 *J. Am. Ceram. Soc.* **79** 3297
[6] Chan W H, Xu Z, Zhang Y, Hung T F and Chen H D 2003 *J. Appl. Phys.* **94** 4563
[7] Fu Z Y, Zhang J C, Hu J H, Jiang Y L, Ding S J and Zhu G D 2015 *Chin. Phys. B* **24** 058502
[8] Fang S X, Tang D Y, Chen Z M, Zhang H and Liu Y L 2015 *Chin. Phys. B* **24** 027802
[9] Berlincourt D, Jaffe H, Krueger H H A and Jaffe B 1963 *Appl. Phys. Lett.* **3** 90
[10] Mirshekarloo M S, Yao K and Sritharan T 2010 *Appl. Phys. Lett.* **97** 142902
[11] Forst D, Li J F and Viehland D 1997 *Appl. Phys. Lett.* **71** 1472
[12] Frederick J, Tan X L and Jo W 2011 *J. Am. Ceram. Soc.* **94** 1149
[13] Wang J F, Yang T Q, Chen S C and Yao X 2014 *Funct. Mater. Lett.* **7** 1350064
[14] Zhang H L, Chen X F, Cao F, Wang G S, Dong X L, Gu Y, He H L and Liu Y S 2010 *J. Appl. Phys.* **108** 086105
[15] Chen X F, Zhang H L, Cao F, Wang G S, Dong X L, Gu Y, He H L and Liu Y S 2009 *J. Appl. Phys.* **106** 034105
[16] Chen X, Hu Z G, Duan Z H, Chen X F, Wang G S, Dong X L and Chu J H 2013 *J. Appl. Phys.* **114** 043507
[17] Li Y, Li Q, Wang L, Yang Z and Chu X 2011 *J. Cryst. Growth* **318** 860
[18] Hao X H, Zhai J W, Kong L B and Xu Z K 2014 *Prog. Mater. Sci.* **63** 1
[19] Zheng Q N, Yang T Q, Wei K, Wang J F and Yao X 2012 *Ceram. Int.* **38** S9
[20] Wang L, Li Q, Xue L H and Liang X M 2007 *J. Mater. Sci.* **42** 7397